



Identification and Localization of Indolent and Aggressive Prostate Cancers Using Multilevel Bi-LSTM

Afnan M. Alhassan¹

Received: 26 November 2023 / Revised: 20 January 2024 / Accepted: 22 January 2024 / Published online: 6 March 2024
© The Author(s) under exclusive licence to Society for Imaging Informatics in Medicine 2024

Abstract

Identifying indolent and aggressive prostate cancers is a critical problem for optimal treatment. The existing approaches of prostate cancer detection are facing challenges as the techniques rely on ground truth labels with limited accuracy, and histological similarity, and do not consider the disease pathology characteristics, and indefinite differences in appearance between the cancerous and healthy tissue lead to many false positive and false negative interpretations. Hence, this research introduces a comprehensive framework designed to achieve accurate identification and localization of prostate cancers, irrespective of their aggressiveness. This is accomplished through the utilization of a sophisticated multilevel bidirectional long short-term memory (Bi-LSTM) model. The pre-processed images are subjected to multilevel feature map-based U-Net segmentation, bolstered by ResNet-101 and a channel-based attention module that improves the performance. Subsequently, segmented images undergo feature extraction, encompassing various feature types, including statistical features, a global hybrid-based feature map, and a ResNet-101 feature map that enhances the detection accuracy. The extracted features are fed to the multilevel Bi-LSTM model, further optimized through channel and spatial attention mechanisms that offer the effective localization and recognition of complex structures of cancer. Further, the framework represents a promising approach for enhancing the diagnosis and localization of prostate cancers, encompassing both indolent and aggressive cases. Rigorous testing on a distinct dataset demonstrates the model's effectiveness, with performance evaluated through key metrics which are reported as 96.72%, 96.17%, and 96.17% for accuracy, sensitivity, and specificity respectively utilizing the dataset 1. For dataset 2, the model achieves the accuracy, sensitivity, and specificity values of 94.41%, 93.10%, and 94.96% respectively. These results surpass the efficiency of alternative methods.

Keywords Multilevel Bi-LSTM · ResNet-101 · Channel-based attention module · Spatial attention module · And Prostate cancers

Introduction

Prostate cancer is one of the prevalent malignancies affecting men, marked by the abnormal proliferation of cells. If left untreated, these anomalous tissues can undergo uncontrolled expansion, with the potential to metastasize to various parts of the body [19]. While prostate cancer can exhibit rapid growth and spread, it often follows a slow progression in most cases. Year by year, an increasing number of men receive this diagnosis [10]. Accurately diagnosing prostate cancer can pose challenges due to the risk of incorrect

results and the discomfort associated with diagnostic procedures. Given its higher incidence in older men, there is a pressing need for a precise classification methodology [4]. Prostate cancer ranks as the fourth most common cancer globally [16]. An advanced stage of this cancer is metastatic castration-resistant prostate cancer, known for its resistance to androgen deprivation therapy. In its initial stages, this disease frequently presents with no noticeable symptoms, underscoring the significance of active surveillance before considering treatment options [11]. Despite the complexities in diagnosing its various stages, determining the appropriate treatment pathway can be a formidable task [8]. Methods employed for detecting prostate cancer in its early stages include antigen measurement and digital rectal examinations. When test results point toward the presence of prostate

✉ Afnan M. Alhassan
aalhassan@su.edu.sa

¹ College of Computing and Information Technology, Shaqra University, 11961 Shaqra, Saudi Arabia

cancer, a biopsy is typically recommended for these patients [7, 14].

CorrSigNIA is a diagnostic method used in the assessment of prostate cancer, comprising two key modules: feature learning and detection [23]. Features are initially trained and subsequently extracted by passing through convolutional and RELU blocks. VGG-16 network is employed for feature extraction from MRI images [18]. This approach involves a correlation study of feature space and the extracted features. Deep learning (DL), a cutting-edge technique in artificial intelligence, has gained significant traction across various domains [21]. In ANN, computations are performed by neurons, serving as the fundamental computational units. Neurons are grouped into multiple layers, with data from one layer being transmitted to the next layer. This forms a layered structure, allowing for complex information processing [4, 17]. The CNN utilizes three MRI images, namely T2-weighted diffusion coefficient and diffusion-weighted images. Due to the relatively small image size, both down-sampling and up-sampling techniques are employed for prostate cancer detection [5, 6]. The data processing approach encompasses signal segmentation, and the power spectral analysis is carried out utilizing the Welch method. Additionally, a Hamming window of 2500 sampling points in length is applied. An automated learning procedure is integral to parameter estimation in the CNN [2]. The learning rate is dynamically adjusted after numerous iterations, contributing to improved training performance [3]. For sample classification, linear analysis is employed, and depending on the disease's progression, these samples can be summarized into a single value [13, 20].

During the testing phase, predictive probabilities are transformed into discrete classes, assigning a class based on the normalized probability value. This approach facilitates effective feature extraction and data analysis, catering to the unique challenges posed by disease detection and classification [15, 22]. The combination of power spectral measurement, windowing techniques, and automated learning aids in optimizing the performance of the CNN. It enables accurate categorization of samples, particularly in the context of disease progression. The incorporation of discriminant analysis adds to the overall efficiency by reducing the dimensionality of wavelength data [1]. This streamlined process enhances the accuracy and reliability of predicting disease presence, contributing to improved diagnostic capabilities [24] [12]. The conventional techniques involve limitations as the detection depends on ground truth labels with limited accuracy, and histological similarity, and neglects the disease pathology characteristics found in resected tissue. Further, the subtle differences found in the appearance of the cancerous and healthy tissue introduce more false positive and false negative predictions. Additionally, it is more challenging to localize and distinguish the indolent and aggressive cancer types

when they co-exist within the mixed lesion which occurs generally in 48% of all cancers and 76% of index lesions [6].

To overcome the above limitations, the research presents a robust framework that can accurately identify and pinpoint both slow-growing and aggressive prostate cancers by employing a multilevel Bi-LSTM model. The technique commences with MRI-based image collection from Prostate158—Training data and the Prostate MRI dataset, followed by rigorous pre-processing and ROI extraction. These pre-processed images are subjected to multilevel feature map-based U-Net segmentation, fortified with ResNet-101 and a channel-based attention module for enhanced performance. Segmented images undergo feature extraction, including statistical and hybrid-based features. Extracted features are then fed into the multilevel Bi-LSTM model, optimized further with channel and spatial attention mechanisms. The contributions are as follows:

Multilevel Bi-LSTM for prostate cancer detection The localization of indolent and aggressive prostate cancer involves the multilevel feature map-based U-Net, an encoder-decoder segmentation network with skip connections for obtaining the precise delineation of structures that provides the effective segmentation of medical imaging, including prostate cancer analysis. By utilizing feature maps at different scales, it captures both fine and coarse details, enhancing segmentation accuracy. The advantages include improved localization and recognition of complex structures, such as tumors within prostate images. Further, the channel attention and spatial attention enabled BiLSTM is utilized in the model to learn the bidirectional long-term dependencies that exist in the sequential features to provide the effective identification and localization of prostate cancer.

The manuscript is structured as follows: In “[Literature Review](#)” an overview of existing methods for detecting prostate cancer and their limitations is presented. “[Proposed Methodology for Recognizing and Detecting Aggressive and Slow-Growing Prostate Tumors](#)” delves into the multilevel Bi-LSTM model, providing a detailed explanation of its mathematical foundations. The results and insights derived from the application of the multilevel Bi-LSTM model are outlined in “[Results and Discussion](#)”. Lastly, “[Conclusion](#)” serves as the concluding part of this phase, summarizing the key findings and contributions of this study.

Literature Review

The following is an evaluation of prostate cancer detection techniques: A DL framework for the identification of prostate tumors in consecutive contrast-enhanced ultrasound images was developed by Feng et al. [1]. The technique

significantly improved diagnostic accuracy by capturing dynamic perfusion information using three-dimensional convolution processes. However, the method's effectiveness depends on the availability of contrast agents, which could limit its applicability in cases where these agents are inaccessible or contraindicated due to patient-specific factors or allergies. Iqbal et al. [2] explored a range of deep learning techniques (LSTM and ResNet-101) alongside traditional hand-crafted features, comparing various classifiers. LSTM achieved high sensitivity and accuracy, while ResNet-101 demonstrated exceptional performance with 100% accuracy. These approaches led to enhanced diagnostic accuracy, but deep learning methods may demand substantial computational resources and extensive data. A machine learning (ML)-enabled computer-aided diagnostic approach was presented by Arif et al. [3] and was created especially to detect and classify serious prostate tumors in low-risk individuals who are actively being monitored. This method contributed to improved diagnostic accuracy and assisted in the objective assessment of MRI images, particularly for low-grade tumors. The method achieved commendable sensitivity and specificity, facilitating objective MRI image assessment for low-grade tumors. While this approach improved diagnostic accuracy, potential drawbacks include the need for specialized equipment and expertise for implementation. Addressing the diagnostic challenges posed by prostate cancer in the US, Abbasi et al. [4] employed robust GoogleNet and traditional ML methods for detection. DL outperformed other methods, delivering promising results. Enhanced accuracy was a notable advantage, but deep learning techniques might require substantial computational resources and extensive data. Prostate cancer diagnostic models were introduced by Chen et al. [5] using photoacoustic physio-chemical spectra collected from both healthy and malignant prostate tissue. This innovative approach allowed for non-invasive diagnostic techniques, showing great potential for the early detection of prostate cancer. The non-invasive approach held promise for early cancer detection, yet challenges included data quality and the complexity of implementing ML techniques. Bhattacharya et al. [6] presented CorrSigNIA, a fusion model that uses pathology and radiology data to identify and pinpoint prostate cancer on MRI with precision. This method improved diagnostic precision and the ability to distinguish between indolent and aggressive cancer. Challenges included the need for access to both MRI and pathology data for training and implementation. de Vente et al. [7] introduced NN capable of simultaneously detecting and grading cancer tissue, offering a clinically relevant approach. Their model outperformed standard classification and regression methods, but limitations included the requirement for a specific dataset and potential challenges in generalizing to broader clinical settings. Broomfield et al. [8] presented the use of ISFETs in a point-of-care clinical diagnostics

platform for detecting prostate cancer-related mRNA markers with high sensitivity and specificity. This technology enabled rapid detection within 30 min, potentially advancing early cancer diagnosis. However, practical implementation and scalability for widespread clinical use may necessitate further validation and optimization. Gavade et al. [29] introduced a DL approach involving the U-Net architecture for segmenting ROI and an LSTM model for classifying the ROI to detect prostate cancer. The validation reduced the bias and enhanced the generalizability that boosts the reliability and fosters clinical adoption of CAD systems. Furthermore, the method can be extended by integrating vision transformers (ViTs) and CNNs for cancer grading tasks in the future. Alshareef et al. [30] utilized microarray gene expression data in which the chaotic invasive weed optimization (CIWO) was utilized for selecting the optimal subset of features. Further, DNN classified the features to detect the presence of cancer and eliminated the computational complexity as well as enhanced the detection accuracy. Furthermore, hybrid DL-enabled prediction models integrated with metaheuristics optimizers can be included to enhance the detection results. Moroianu et al. [18] suggested a extraprostatic extension (EPE) detection on multiparametric MRI, in which the trained DL models were employed that generated the cancer probability maps both inside and outside the prostate. Further, the image post-processing pipeline generated the predictions for EPE location concerning the probability maps. However, the technique generated multiple EPE false positives due to the anatomical features outside the prostate. Future work will concentrate on increasing the cohort size and validation as well as enhanced strategies for reducing false positives. Kassem et al. [36] presented a transfer learning (TL) model utilizing the explainable AI framework with ResNet50 for detecting pelvis fractures, in which the GRAD-CAM validated the correct input pelvic segments and localized the fracture regions to enhance the accuracy. However, the technique utilizing ResNet50 and TL model failed to predict three classes, while the technique utilizing TL and GoogleNet model failed to predict one normal and fracture case utilizing the real X-ray images. Eltoukhy et al. [37] utilized the Residual DL model that classified the complex histopathological images. The model reduced the vanishing gradient problem with the RELU unit and offered robust computation. Additionally, the technique reduced the computation complexity and classified up to eight classes of breast cancer types. Naguib et al. [38] introduced the Pre-Trained Model AlexNet and GoogleNet model for predicting cervical spine fractures. The technique utilized the saliency map to evaluate the spatial support of a specific class within the image. Further, the technique classified 68 unlabeled X-ray images and offered low cost for implementation. However, some challenges associated with the design and selection bias are found that reduced the generalizability of

the model. Alshahfi et al. [39] presented the deep residual network that utilized multiple filters for multilayer feature extraction. The technique overcame the imbalanced dataset issue by transforming the dataset into image and weight vectors. Further employing the various filter sizes protected the model from overfitting issues. However, the drawbacks such as high running time limited the performance and the technique cannot be executed in microdevices with limited memory.

Challenges

- To enhance the diagnosis of prostate cancer utilizing the clinical CESUS data, the development of advanced deep learning models is imperative, particularly when dealing with larger datasets.
- Improving both the accumulation of additional samples and the refinement of classification models is vital for achieving higher diagnostic accuracy.
- It is essential to support radiologists in MRI interpretation by leveraging the capabilities of CorrSigNIA. Additionally, exploring the feasibility of applying these models to external data from multiple scanners is a crucial step.
- Tasking radiologists with evaluating the utility of CorrSigNIA in MRI interpretation is a valuable assignment, as it aids in understanding its practical benefits.
- While it may be feasible to predict the Grade Group (GGG) based on MRI data, it is currently not possible to perform a similar grading from pathology images. This distinction is worth noting.

The multilevel Bi-LSTM utilizing multilevel feature map-based U-Net for prostate cancer detection overcame the above limitations of existing techniques. The multilevel Bi-LSTM technique provides the advantage of capturing spatial information and context at the same time. The end-to-end pipeline process directly generates the segmentation maps and preserves the full context of the MRI images reducing the computational complexity. Further, the BiLSTM effectively predicts the features available to the network and improves the information of the cancer localization to effectively detect prostate cancer.

Proposed Methodology for Recognizing and Detecting Aggressive and Slow-Growing Prostate Tumors

The key intention of this research is to develop a resilient framework that enables the accurate identification and localization of both indolent and aggressive prostate cancers. This is achieved through the utilization of a multilevel Bi-LSTM

model, which enhances the precision of the diagnostic process. The research workflow commences with the procurement of MRI-based prostate cancer images from the Prostate158—Training data [9] and the Prostate MRI dataset [10]. This is followed by a series of essential steps, including pre-processing and ROI extraction. Subsequently, the pre-processed images undergo a multilevel feature map-based UNet segmentation process. To enhance performance, ResNet-101 and a channel-based attention module are judiciously integrated into the segmentation process. The resulting segmented images are then subjected to feature extraction, encompassing a range of components such as statistical features, a global hybrid-based feature map, and the generation of a feature map using ResNet-101. Once the features are extracted, they serve as inputs to the multilevel Bi-LSTM model. Additional enhancements are introduced via the incorporation of channel attention and spatial attention mechanisms. The model's performance is rigorously evaluated by subjecting it to an independent test dataset, and its classification output is meticulously analyzed using key metrics, including accuracy, sensitivity, and specificity. Figure 1 serves as a visual representation of the developed framework, offering a comprehensive overview of the research approach. The ultimate objective is to notably enhance the precision and dependability of prostate cancer identification and localization, encompassing both indolent and aggressive variations of the condition.

Input

The dataset utilized in this research is sourced from the Prostate 158—Training data and the Prostate MRI dataset. It serves as a valuable resource in the domain of identifying and localizing both indolent and aggressive prostate cancers, comprising a diverse collection of MRI-based prostate cancer images. The mathematical representation of this dataset can be expressed as follows,

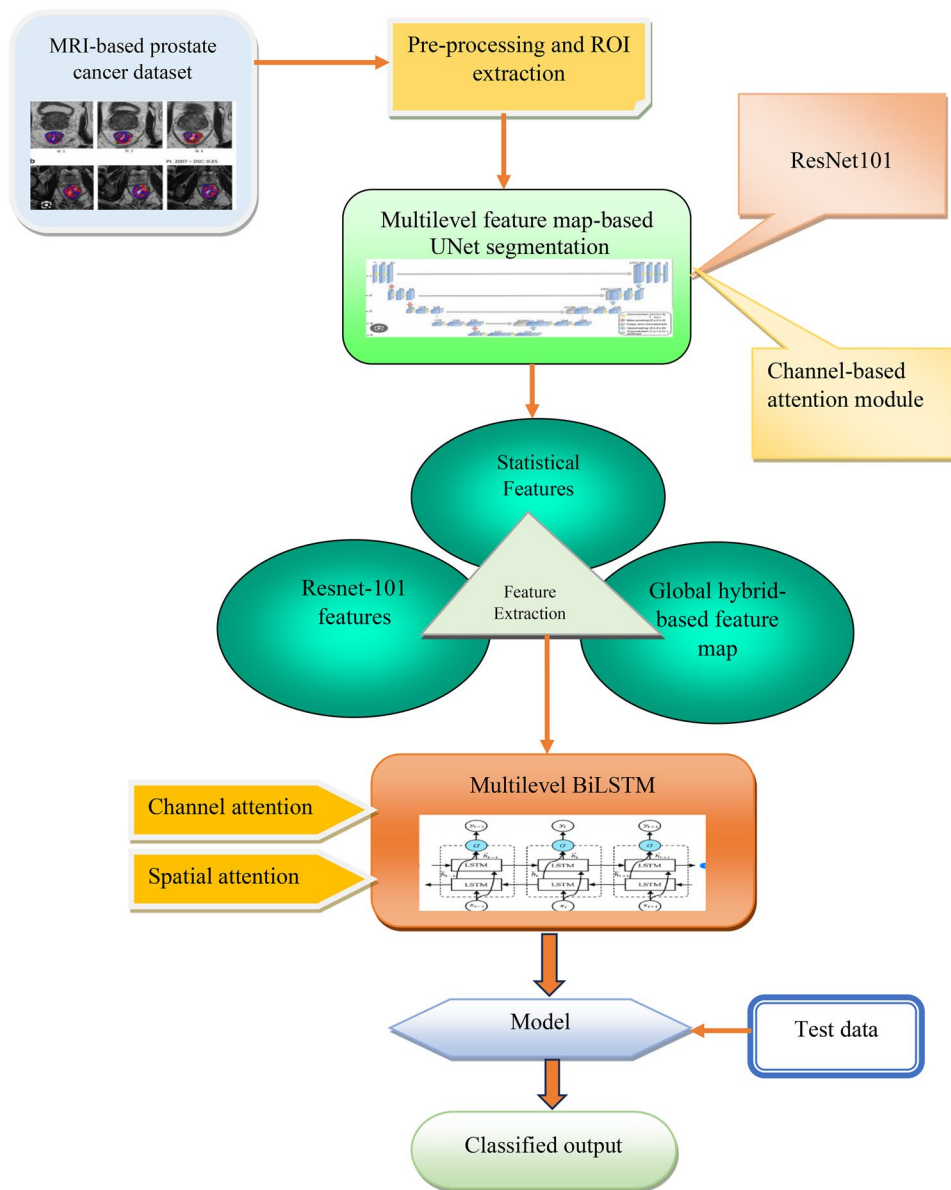
$$C = \sum_{a=1}^g C_a + \sum_{b=1}^k C_b \quad (1)$$

where the Prostate dataset is denoted as C , and C_a denotes the Prostate 158—Training data images, which range from 1 to g ; C_b denotes the Prostate MRI dataset images, which varies from 1 to k .

Pre-processing and ROI Extraction

The pre-processing of prostate cancer images is a vital series of steps designed to enhance image quality and facilitate precise analysis. An integral facet of this process is the removal of noise, which serves to eliminate unwanted artifacts or distortions present in the images. The benefits of pre-processing are manifold, including heightened image clarity, improved

Fig. 1 Block diagram representation of the proposed method



feature extraction, and enhanced interpretability. These improvements, in turn, lead to more accurate detection and diagnosis of prostate cancer. Pre-processing techniques, particularly noise reduction, play a pivotal role in ensuring that medical professionals can make reliable decisions based on the images, ultimately elevating the quality of patient care and treatment outcomes. Following pre-processing, the ROI is meticulously extracted by segmenting the prostate region from the surrounding tissues. This is often achieved through techniques such as thresholding or contour detection. The extraction of the ROI is instrumental in isolating the prostate gland for thorough analysis, a critical aspect of accurate diagnosis and treatment planning. By minimizing interference from irrelevant areas, it results in clearer and

more focused data for analysis. This focused approach not only enhances precision but also reduces the computational load, expediting the analysis and making it more efficient. In mathematical terms, this process can be expressed as,

$$C^* = \sum_{a=1}^g C_a^* + \sum_{b=1}^k C_b^* \tag{2}$$

where C^* denotes the pre-processed dataset images.

Multilevel Feature Map-Based U-Net Segmentation

After pre-processing the images are passed through a multilevel feature map-based U-Net segmentation process, with

performance enhancement achieved through the utilization of ResNet-101 and a channel-based attention module. A multilevel feature map-based U-Net segmentation is an advanced image segmentation technique used in medical imaging, including prostate cancer analysis. It employs a modified U-Net architecture with multiple levels of feature maps, allowing for the precise delineation of structures. The advantages include improved localization and recognition of complex structures, such as tumors within prostate images. By utilizing feature maps at different scales, it captures both fine and coarse details, enhancing segmentation accuracy. This approach aids in automated diagnosis, treatment planning, and monitoring, ultimately leading to more effective and efficient healthcare, reducing manual effort, and improving patient outcomes in prostate cancer management.

U-Net Model

The U-Net model functions as an end-to-end semantically segmented network and is named for its symmetrical U-shaped structure. It comprises essential architectural components, including an input layer, convolutional layers, pooling layers, transposed convolutional layers, activation functions, and an output layer. Within the convolution layer, multiple 3×3 convolution kernels are employed with a stride of 1, resulting in the creation of a feature map. An important feature of this convolution operation is weight sharing, where the same set of weights is applied to all input data. By drastically lowering the number of trainable parameters, this weight-sharing technique improves computing efficiency. Furthermore, convolution introduces the advantageous attribute of local perception, enhancing the neural network's ability to capture spatial information. The activation function is an essential component in increasing the non-linearity of the neural network, enabling it to better approximate nonlinear mappings and enhance model expressiveness. Activation functions are pivotal in neural network architectures, with common choices including sigmoid, Tanh, and rectified linear unit (ReLU). Within the U-Net model, the ReLU activation function is the preferred choice. Mathematically, the ReLU activation function can be defined [33] as follows:

$$RELU = \begin{cases} y & y \geq 0 \\ 0 & y < 0 \end{cases} \quad (3)$$

The unique feature of the ReLU activation function is its ability to suppress negative values by transforming inputs greater than zero into positive values and reducing those less than zero to zero. This property speeds up the training of the network by transforming dense features into sparser ones, which improves feature robustness. To improve linear differentiability, the sparse features are converted into a

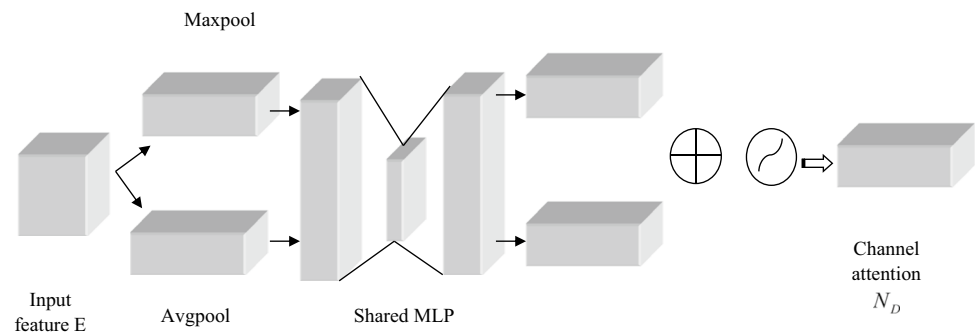
higher-dimensional space. Fundamentally, transposed convolution is about upsampling; it is a series of processes that return the feature map to its original dimensions of the image. With the introduction of skip connections, the U-Net model improves the network's capacity for effective generalization while keeping information at each level. Concatenation is used to combine the up-sampled feature channel dimension with the downsampled feature channel dimension, integrating contour information with detailed image information. Using a 1×1 convolution kernel, this fusion method maps feature vectors to the required number of classes. The loss function sometimes referred to as the optimization performance metric measures how similar predicted values are to the ground truth and uses this information to determine how to optimize the neural network's weights. When it comes to U-Net, its loss function is the boundary loss [33], which is described as,

$$F = \sum_{Y \in \Omega} \omega(y) \log_{l(y)} y \quad (4)$$

where $l(y)$ is the loss function of softmax and $l : \Omega \rightarrow \{1, 2, \dots, h\}$ is the pixel point's label value.

Channel-Based Attention Module

A channel-based attention module is a neural network component designed to selectively enhance or suppress feature maps (channels) within intermediate layers. Its purpose is to focus on relevant information while disregarding noise. When integrated into a multilevel feature map-based U-Net segmentation process, the channel-based attention module significantly improves feature discrimination and reduces noise. This integration combines the segmentation capabilities of U-Net with feature-focused attention, resulting in a segmentation model that is more accurate, robust, and efficient. This enhancement strengthens the network's ability to precisely delineate structures such as prostate tumors in medical images, contributing to more accurate diagnosis and treatment planning. For a more efficient feature map generation, the introduction of channel attention proves pivotal in adaptively extracting informative features before reaching the maximum pooling layer. The channel attention mechanism operates through the following steps: It generates a feature map denoted as GBD, derived from global average pooling $E_{avg}^D (1 \times 1 \times D)$ and global maximum pooling $E_{max}^D (1 \times 1 \times D)$. These E_{avg}^D and E_{max}^D values undergo processing within a shared network comprising an activation layer and two fully connected (FC) layers. After going through the shared network, the results of E_{avg}^D and E_{max}^D are combined using the Add function and then run through the sigmoid function to produce an attention channel map $N_D \in S^{1 \times 1 \times D}$. The size of the second FC layer is restored to $S^{1 \times 1 \times D}$, while the size of the first FC layer is determined as $S^{1 \times 1 \times D/r}$. Figure 2 shows a graphic illustration of the channel attention module.

Fig. 2 Channel attention module

Resnet-101

ResNet-101 is a deep CNN architecture comprising a remarkable 101 layers, celebrated for its capability to effectively train very deep neural networks [34]. When integrated into a multilevel feature map-based U-Net segmentation process, the inclusion of ResNet-101 significantly amplifies feature extraction and representation. This augmentation empowers the network to capture intricate patterns within medical images with greater precision. The amalgamation of ResNet-101 harnesses its robust feature extraction capabilities, resulting in the development of more accurate and resilient segmentation models. This synergy notably elevates segmentation accuracy, enabling the precise identification of structures like prostate tumors. Consequently, this contributes to more accurate diagnosis and treatment planning while concurrently reducing false positives in medical imaging. ResNet-101 boasts a neural network architecture that encompasses a series of convolutional layers, denoted as conv1, conv2_y, conv3_y, conv4_y, and conv5_y, complemented by pooling, fully connected, and softmax layers. Its distinction lies in its profound depth of convolutional layers, achieved through the ingenious implementation of shortcut connections. These shortcuts facilitate identity mapping, effectively mitigating the degradation problem commonly associated with exceedingly deep networks. Notably, these connections introduce no additional parameters or computational complexity. Another distinctive feature that distinguishes the ResNet-101 model is its capability for end-to-end training facilitated by stochastic gradient descent and back-propagation, ultimately leading to superior performance. This architecture adeptly addresses challenges related to network depth while maintaining computational efficiency.

Feature Extraction

The resulting segmented images then undergo feature extraction, encompassing statistical features, a global hybrid-based feature map, and a ResNet-101 feature map generation step. Feature extraction in prostate cancer image analysis is the

process of identifying and quantifying relevant visual attributes within medical images, such as texture, shape, or intensity patterns. This is essential because raw medical images can be complex and high-dimensional. Feature extraction reduces data dimensionality, simplifies information, and enables the detection of subtle cancer-related characteristics that may be challenging to discern directly. The advantages include enhanced diagnostic accuracy, more efficient computational processing, and the ability to customize the analysis to specific diagnostic or research requirements, ultimately improving early detection and treatment planning in prostate cancer, which is vital for patient outcomes and care. This research employs a three-pronged approach to feature extraction, encompassing statistical features, the creation of a global hybrid-based feature map, and a ResNet-101 feature map generation step, which is elaborated upon in the following section.

Statistical Features

Statistical features in image analysis involve numerical characteristics including the mean, variance, and standard deviation, capturing information about pixel distribution. They are essential in medical image processing to quantify texture and intensity patterns, aiding in distinguishing between healthy and cancerous tissue. Their advantage lies in providing quantitative, objective data for enhanced precision in cancer identification and localization, reducing subjectivity in diagnosis.

Global Hybrid-Based Feature Map

A global hybrid-based feature map combines both local and global information in image analysis. It integrates local details with overall context, aiding in accurate cancer detection. Its advantage lies in preserving fine-grained local features while considering the broader image context, enhancing the model's ability to discern subtle variations and patterns crucial for prostate cancer identification and localization.

ResNet-101 Feature

ResNet-101 features are deep learning representations extracted from a Residual Network with 101 layers. They capture hierarchical features from images, enabling the model to learn complex patterns. The advantage lies in leveraging pre-trained ResNet-101 features to enhance the accuracy of cancer detection, as they contain valuable hierarchical information, reducing the requirement for manual feature engineering.

Multilevel Bi-LSTM Model

After feature extraction, these extracted features are employed as inputs to the multilevel Bi-LSTM model, where additional enhancements are introduced through the integration of channel attention and spatial attention mechanisms. The LSTM network is a variant of the RNN family. While RNNs are effective in handling time series data, they are limited in their ability to capture long-term dependencies. This limitation stems from their short-term memory, which can hinder their performance on signals with persistent time information. To address this, LSTM networks were introduced, proving particularly adept at solving regression-based problems involving data with extended temporal information. Conventional LSTM models process data in a forward direction, incorporating information from previous moments but not considering future moments. This design poses limitations in handling complex tasks, prompting the development of bidirectional LSTM. Bidirectional LSTM, as the name suggests, leverages both past and future features within a single time step. It is built from a single LSTM cell and functions both forward and backward, allowing for bidirectional information transfer. However, it's crucial to emphasize that a bidirectional LSTM's typical output typically only contains the final time step of the hidden layers. While logical, this output's instability hinders its effectiveness in estimating a continuous joint angle sequence.

Each LSTM unit is composed of four main components: memory cells, forget gates, output gates, and input gates. These gates interact with one another through bias terms and weights, resulting in complex calculations. The following model provides a mathematical expression for the basic memory cell structure (5)–(9) [31],

$$in_t = \sigma(G_{y_{in}}y_t + G_{k_{in}}k_{t-1} + G_{b_{in}}b_{t-1} + a_{in}) \tag{5}$$

$$fo_t = \sigma(G_{y_{fo}}y_t + G_{k_{fo}}k_{t-1} + G_{b_{fo}}b_{t-1} + a_{fo}) \tag{6}$$

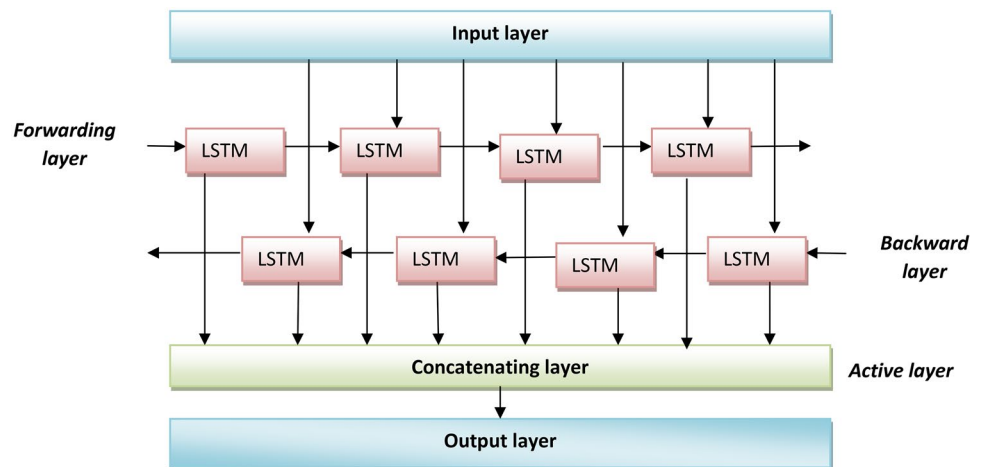
$$b_t = fo_t b_{t-1} + i_t \tanh(G_{y_b}y_t + G_{k_b}k_{t-1} + a_b) \tag{7}$$

$$op_t = \sigma(G_{y_{op}}y_t + G_{k_{op}}k_{t-1} + G_{b_{op}}b_{t-1} + a_{op}) \tag{8}$$

$$k_t = op_t \tanh(b_t) k_{a_{op}} \tag{9}$$

where the input is represented by y , the activation function is denoted by σ , and the cell state vectors, forget gate, input gate, and output gate are denoted by in , fo , op , and b , which all have the same lengths as the hidden vector k . The state at time t or time $t - 1$ is indicated by the vector subscripts. The weight matrix subscripts represent the weight matrix magnitudes. For example, G_{k_b} represents the hidden-cell gate matrix and the input and output gate matrix is represented by $G_{y_{op}}$. As seen in Fig. 3, the Bi-LSTM combines each forward and backward path. The Bi-receptive field LSTMs are greatly increased by this bidirectional information flow. In the forward direction, the cell output at times $t - 1, t, t + 1$ is represented by $k_{f_0}, k_{f_1}, k_{f_2}$, respectively. Similarly, the cell output at the appropriate time steps is represented as $k_{b_0}, k_{b_1}, k_{b_2}$ in the reverse way. As a result, rather than $(k_{f_0}, k_{f_1}, k_{f_2})$, the Bi-LSTM's outputs should be $\{[k_{f_0}, k_{b_2}], [k_{f_1}, k_{b_1}], [k_{f_2}, k_{b_0}]\}$ [32]. The network's information content is improved by this extension. The outputs of

Fig. 3 Bi-LSTM architecture



this study must have a close relationship because the main objective is to determine the ongoing joint angle curve connected to upper limb kinematics. Consequently, every time step and output are routed into the same high-level layer and normalized, so tightly restricting the outputs.

Spatial Attention Module

The spatial attention module is a neural network component designed to selectively emphasize or suppress specific spatial regions within an input feature map. This is particularly valuable in computer vision tasks, where focusing on relevant image regions enhances model performance. In the context of the multilevel Bi-LSTM model, the integration of spatial attention mechanisms improves the model's ability to adaptively highlight essential spatial features within medical images, such as intricate patterns in prostate cancer images. The advantage lies in enhanced feature discrimination, contributing to more accurate segmentation and diagnosis, while reducing false positives, ultimately improving medical imaging outcomes. Initially, we process the input features with $E \in \mathbb{M}^{G \times B \times W}$ channels through batch normalization and ReLU layers, or channel transformation. Here, $E \in \mathbb{M}^{G \times B \times W}$ denotes the number of channel inputs, while B and W represents the height and width of E respectively. Subsequently, we apply two convolution layers with 1×3 and 3×1 kernels to create two new feature maps, $P \in \mathbb{M}^{G \times B \times W}$ and $L \in \mathbb{M}^{G \times B \times W}$. These maps are designed to capture edge information related to tree-like structures, distinguishing between horizontal and vertical orientations. To consolidate these new feature maps, $L \in \mathbb{M}^{G \times B \times W}$ and $L \in \mathbb{M}^{G \times B \times W}$ are reshaped into $\mathbb{M}^{G \times M}$ where $M = B \times W$ signifying the total number of features. A matrix multiplication is then performed to merge the transposed versions of P and L . The application of a softmax layer further allows us to derive spatial associations within the same class [35], facilitating intra-class spatial association,

$$Z_{(x,y)} = \frac{\exp(L_x \cdot P_y^T)}{\sum_{x=1}^M \exp(L_x \cdot P_y^T)} \quad (10)$$

where $Z_{(x,y)}$ denotes the impact of the X^{th} position on the y^{th} position. The feature map undergoes a 1×1 convolution layer to yield a dimension-reduced feature map denoted as $N \in \mathbb{M}^{G \times B \times W}$. The reshaping process converts Z to $\mathbb{M}^{G \times B \times W}$. A matrix multiplication takes place between K and Z resulting in spatial affinities at the pixel level referred to as $N \in \mathbb{M}^{G \times B \times W}$. Finally, we conduct a pixel-level summation of Z and N . This process effectively combines the original impact information with the computed spatial affinities to enhance the final output at the pixel level.

Results and Discussion

The subsequent sections offer an extensive and meticulous examination of the findings and in-depth analysis concerning the developed multilevel Bi-LSTM model's performance in accurately identifying and localizing both indolent and aggressive prostate cancers.

Experimental Setup

The performance evaluation of the multilevel Bi-LSTM model, as well as the comparative analysis of different approaches, was carried out utilizing the Python tool on a Windows 10 operating system, with a computer configuration featuring 8 GB of RAM.

Dataset Description

Prostate158—Training Data (Dataset 1)

Prostate158 is an extensive dataset comprising prostate MRIs that adhere to PI-RADS v2 technical standards and incorporate expert annotations. Alongside a robust baseline algorithm, it serves as an invaluable benchmark for the advancement of cutting-edge algorithms in the field of prostate cancer segmentation and detection.

Prostate MRI Dataset (Dataset 2)

The dataset offers meticulously crafted segmentations by urologic radiology experts, subjected to rigorous review procedures to uphold the highest quality standards. This makes it a valuable resource for researchers in the field of computer vision who may lack direct access to medical data or radiological expertise. They can leverage this dataset to pioneer innovative algorithms for the detection of prostate cancer.

Evaluation Metrics

Accuracy

A diagnostic model's accuracy is a statistic that expresses how accurate its predictions are overall. It calculates the proportion of accurate identifications to all cases in the dataset, including both true negatives and correctly identified cases. Accuracy in the context of prostate tumor identification evaluates the model's capacity to accurately categorize cases that are both indolent and aggressive.

$$acc = \frac{J_m + J_{tp}}{J_m + J_{tp} + J_{fn} + J_{fp}} \quad (11)$$

Sensitivity

The evaluation of the true positive rate gauges how well a diagnostic model can detect instances of a particular ailment such as aggressive prostate cancer is known as sensitivity. It measures how well the model identifies cases of aggressive cancer by dividing the total number of real positive cases by the ratio of true positives,

$$sen = \frac{J_{tp}}{J_{tp} + J_{fn}} \quad (12)$$

Specificity

The capacity of a model to accurately rule out situations without the relevant condition is measured by its specificity. Regarding prostate cancer, it evaluates how well the model classifies patients as indolent when they do not show signs of aggressive cancer. The ratio of genuine negatives to all actual negative situations is used to compute specificity.

$$spec = \frac{J_{tn}}{J_{tn} + J_{fp}} \quad (13)$$

Experimental Results

The experimental results of identifying and localizing aggressive and indolent prostate tumors using the multilevel Bi-LSTM model are illustrated in Fig. 4, which comprises the input image, the pre-processed image, the ROI image, and the segmented image.

and the segmented image. These images are presented to facilitate a comprehensive analysis, enabling an in-depth assessment of the detection and localization process.

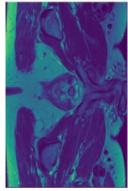
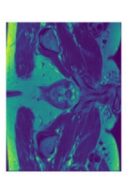

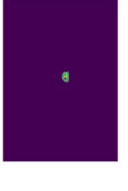
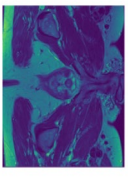
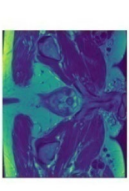

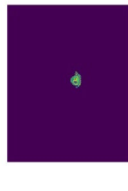
Performance Evaluation

To showcase the effectiveness of the multilevel Bi-LSTM model, performance evaluations are carried out at various epochs, including 100, 200, 300, 400, and 500. These assessments involve the measurement of TP, allowing us to track the performance of the model and its evolution across different time points.

Performance with TP for Dataset 1

The multilevel Bi-LSTM model, intended for the diagnosis and localization of both benign and malignant prostate tumors, shows its accuracy results for dataset 1 in Fig. 5. When assessing accuracy for TP at the 90% threshold, the multilevel Bi-LSTM model achieves the following values: 91.57%, 94.33%, 95.08%, 96.11%, and 96.72%. Similarly, when evaluating sensitivity for TP at the 90% threshold, the model attained the following values: 91.66%, 94.21%, 94.35%, 94.68%, and 96.17%. Additionally, in measuring specificity for the training dataset at the 90% threshold, the proposed multilevel Bi-LSTM achieves the following values: 93.95%, 95.29%, 95.76%, 95.96%, and 96.17%. These results demonstrate the model's consistent improvement in accuracy, sensitivity, and specificity.

Fig. 4 Experimental results of the developed multilevel Bi-LSTM model

Input image	Pre-processed	ROI	Segmented
			
			

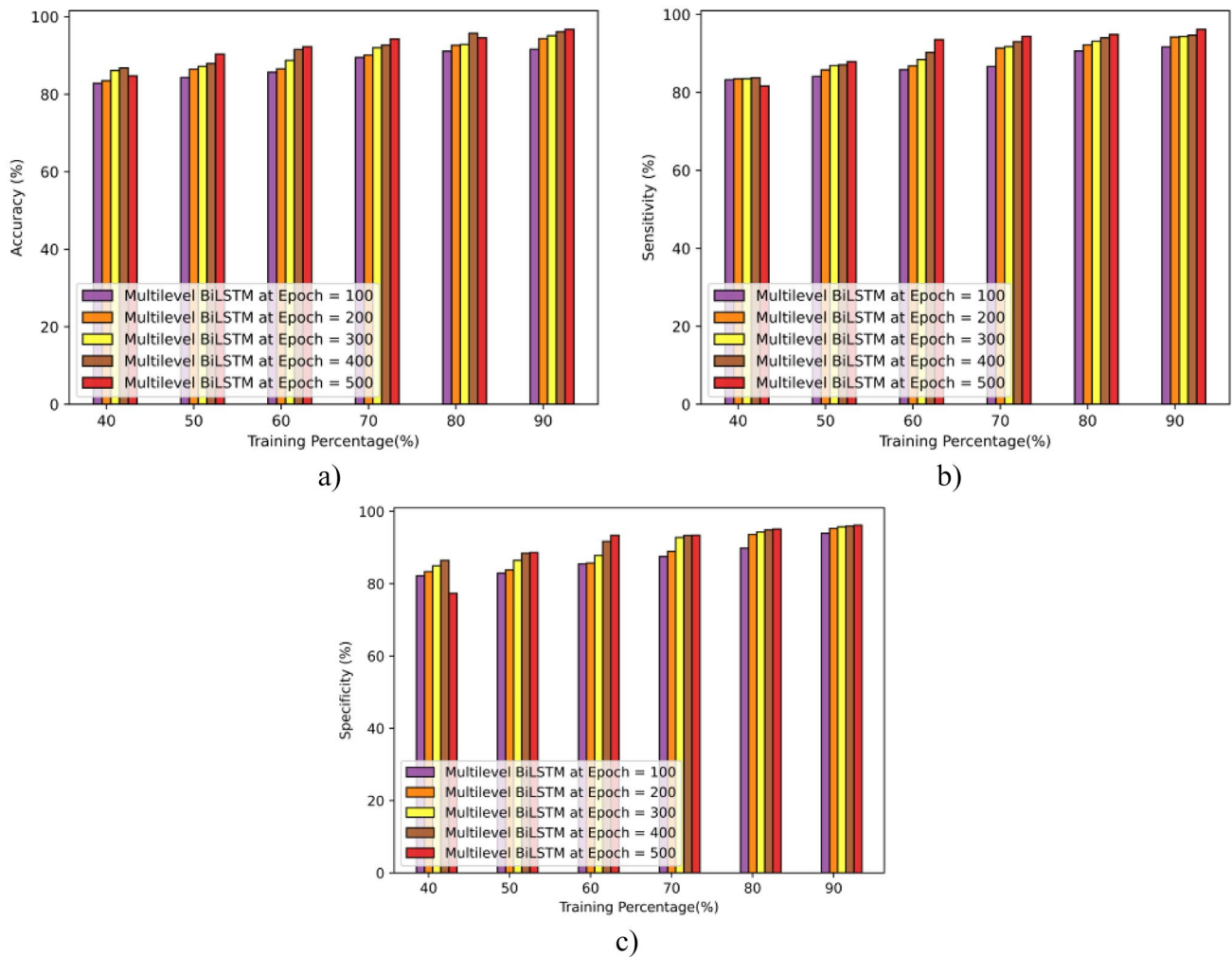


Fig. 5 Performance with TP for dataset 1

Performance with TP for Dataset 2

The multilevel Bi-LSTM model, intended for the diagnosis and localization of both benign and malignant prostate tumors, shows its accuracy results for dataset 2 in Fig. 6. The multilevel Bi-LSTM model achieves the accuracy values of 91.28%, 92.97%, 93.69%, 93.82%, and 94.41% for TP at the 90% threshold. Similarly, when assessing sensitivity at the 90% threshold, the model attained the following values: 92.61%, 92.98%, 92.85%, 92.80%, and 93.10%. Furthermore, when measuring specificity for the training dataset at the 90% threshold, the multilevel Bi-LSTM model achieves the following values: 91.66%, 92.54%, 93.98%, 94.27%, and 94.96%. These results illustrate the model's consistent enhancement in terms of metrics.

Comparative Techniques

The developed multilevel Bi-LSTM model is compared with conventional techniques such as CorrSigNIA [6], Machine Learning [25], Hierarchical Attention NN [26], LSTM [27], and DCNN [28] to evaluate the efficacy of the model.

Comparative Evaluation with TP for Dataset 1

Figure 7 presents a comparative analysis of performance metrics concerning the diagnosis and localization of both benign and malignant prostate tumors, with a focus on dataset 1. While assessing the accuracy, the multilevel Bi-LSTM model exhibits a remarkable increase of 27.61% compared

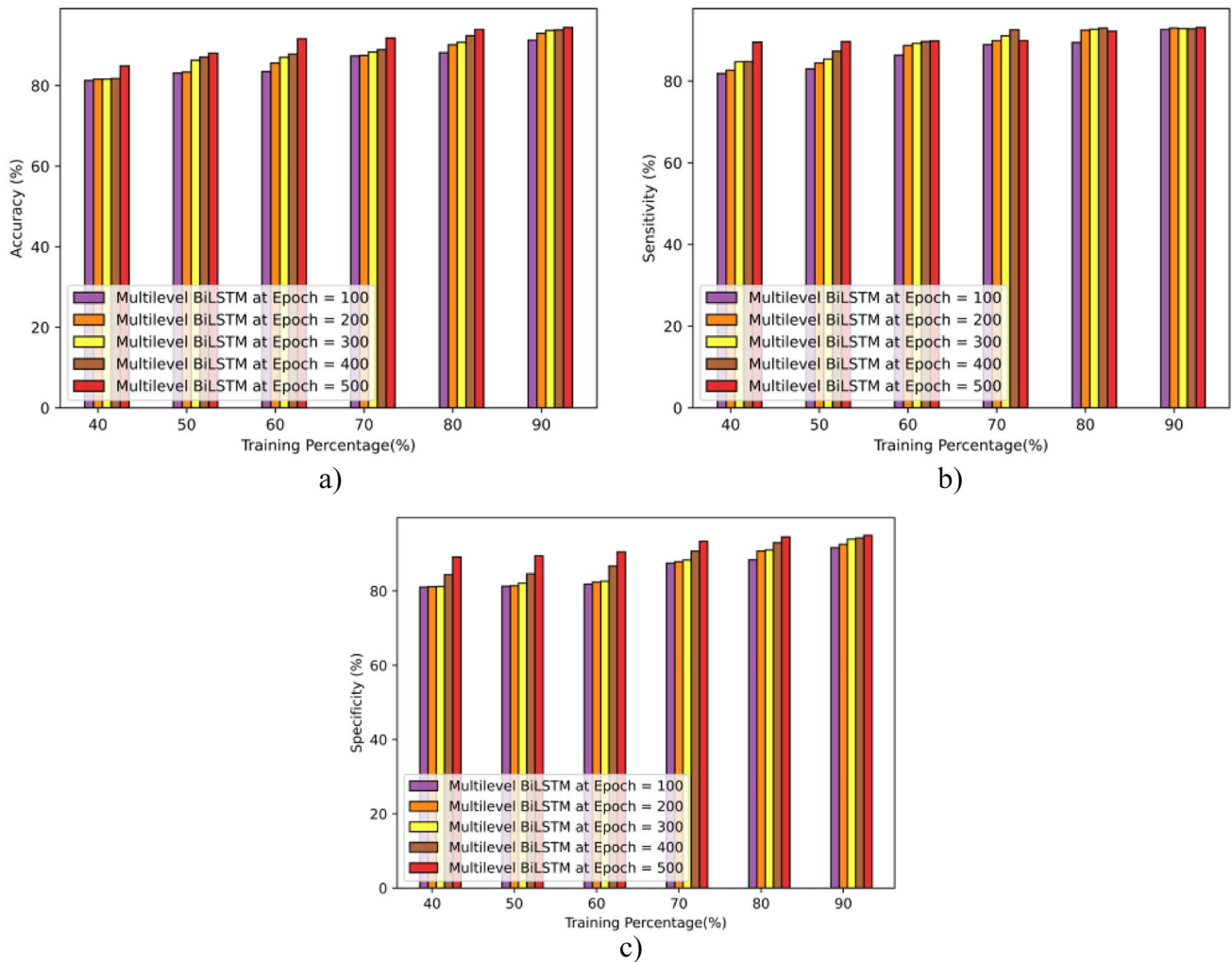


Fig. 6 Performance evaluation with TP for dataset 2

to DCNN for the training dataset at the 90% threshold. The evaluation of sensitivity for the training dataset at the 90% threshold, the multilevel Bi-LSTM model demonstrates a substantial gain of 13.77% when compared to DCNN. Additionally, the specificity of the multilevel Bi-LSTM in the training dataset at the 90% threshold surpasses DCNN, achieving a notable improvement of 5.52%. The analysis reveals the significant efficacy of the multilevel Bi-LSTM model in terms of metrics when contrasted with DCNN.

Comparative Evaluation with TP for Dataset 2

Figure 8 provides a comparative evaluation of performance metrics related to the diagnosis and localization of both benign and malignant prostate tumors, with a specific focus on dataset 2. While concerning the accuracy, the multilevel Bi-LSTM model demonstrates a remarkable improvement

of 32.29% compared to DCNN for the training dataset at the 90% threshold. Additionally, when considering sensitivity for the training dataset at the 90% threshold, the multilevel Bi-LSTM model showcases a substantial boost of 24.59% than the DCNN model. Moreover, in the assessment of specificity for the training dataset at the 90% threshold, the multilevel Bi-LSTM model surpasses DCNN with an impressive gain of 30.02%. These findings highlight the multilevel Bi-LSTM model's notable performance advantages over DCNN, especially when compared in terms of performance metrics.

Comparative Discussion

Most of the conventional techniques exhibit specific challenges in prostate cancer detection and the CorrSigNIA method [6], in which exploring the feasibility of applying

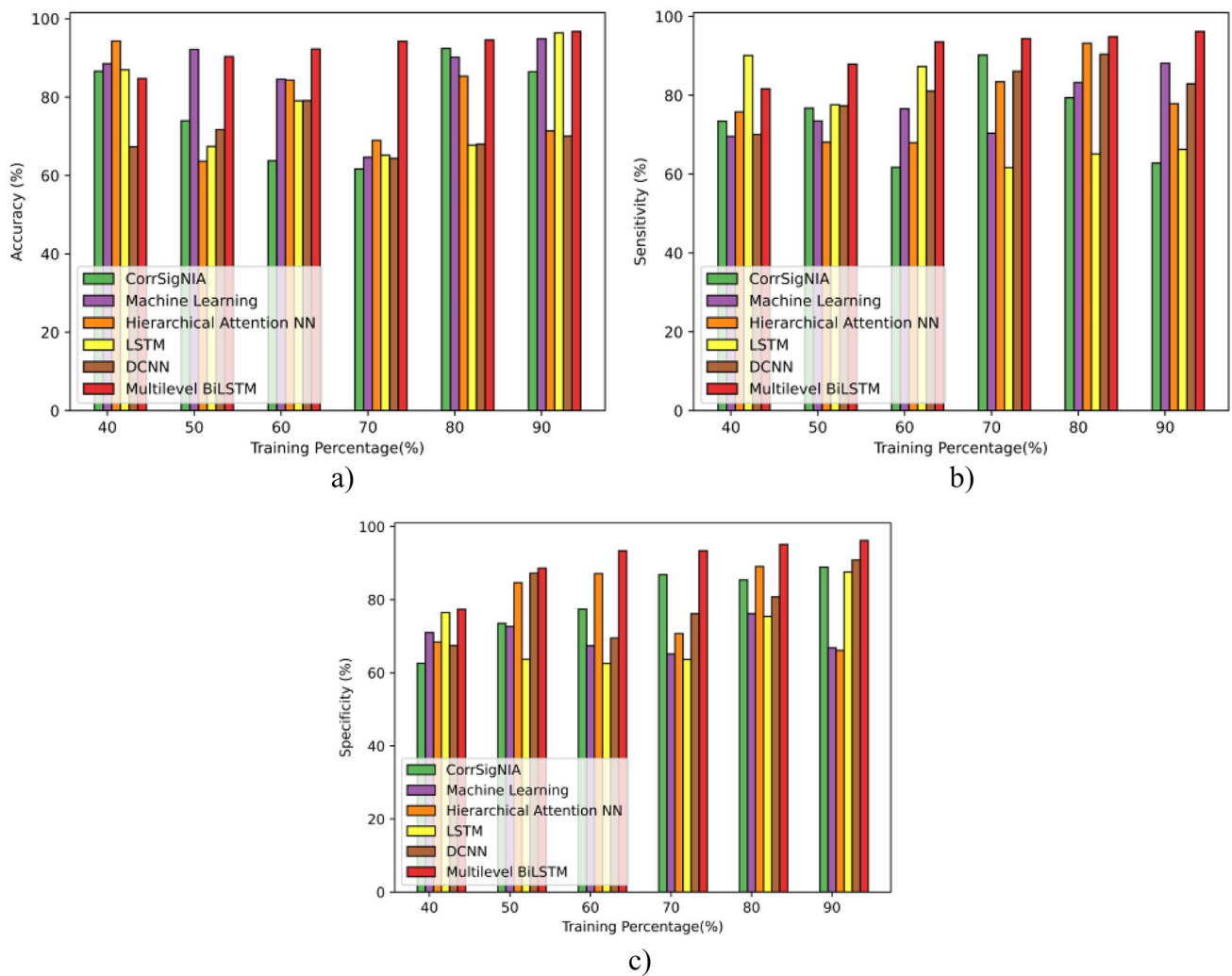


Fig. 7 Comparative evaluation with TP for dataset 1

these models to external data is a crucial step that limits the performance. The LSTM model [27] required integrating vision transformers (ViTs) and CNNs for cancer grading which formed the limitation of the model. Additionally, the DCNN model [28] in which training images and epochs are utilized requires other hyperparameters to be included in the model. Further, the ML model failed to capture the informative features that limited the performance [25]. However, the multilevel Bi-LSTM overcame the above limitations and utilized the multilevel feature map-based U-Net segmentation, fortified with ResNet-101 and a channel-based attention module for enhanced performance. The extracted features containing information such as texture, shape, or intensity patterns are fed to the multilevel Bi-LSTM model for effective classification. Further, the multilevel BiLSTM model optimized through channel

and spatial attention mechanisms provided the effective localization of cancer tissues. The generated segmentation maps preserved the full context of the MRI images and eliminated the complexity of detection. Finally, the multilevel BiLSTM utilizing the long-term dependency prediction improves the information of the cancer localization to effectively detect prostate cancer with high accuracy. However, the developed model sometimes found complexity in calculating the negative and positive values due to the high prevalence of the complex patterns formed with the selection of patient samples.

This section discusses a comparative analysis of diverse methodologies, thoughtfully organizing the data into structured tables for the assessment of TP. The multilevel Bi-LSTM approach emerges as a standout performer, demonstrating exceptional outcomes through precise calibration of

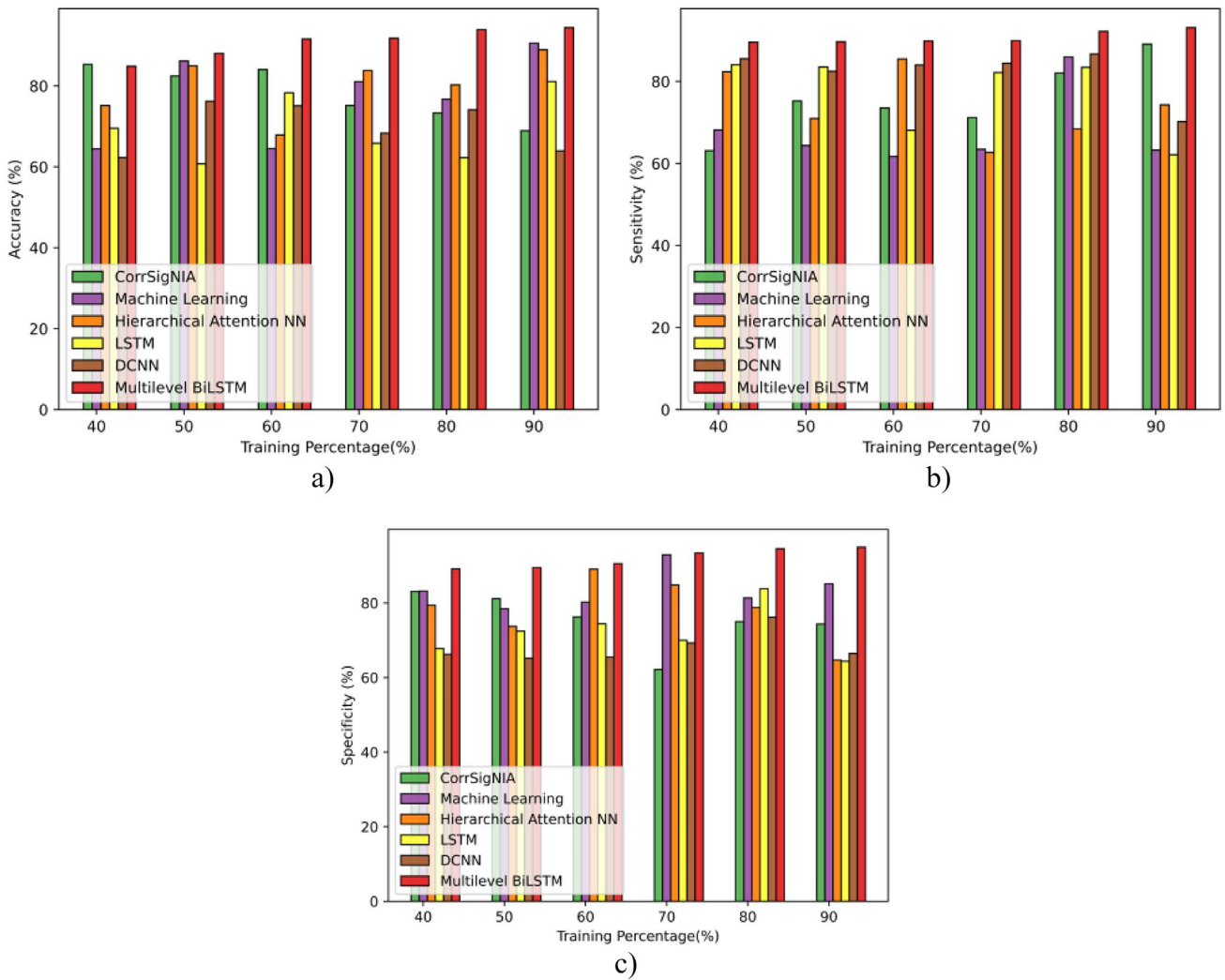


Fig. 8 Comparative evaluation with TP for dataset 2

weights and bias of the classifier. As elucidated in Table 1, we undertake a comparative study, pitting the proposed multilevel Bi-LSTM against contemporary techniques. This assessment is conducted under a consistent 90% TP for equitable evaluation.

Confusion Matrix

The confusion matrix of the multilevel Bi-LSTM model for dataset 1 is depicted in Fig. 9, which shows that the model predicted precisely. In Fig. 9a, the true labels and predicted

Table 1 Comparison discussion for datasets 1 and 2

Methods/metrics	Training percentage (TP) 90					
	Dataset 1			Dataset 2		
	Acc (%)	Sen (%)	Speci (%)	Acc (%)	Sen (%)	Speci (%)
CorrSigNIA	86.48	62.80	88.91	68.91	89.08	74.33
Machine Learning	94.90	88.13	66.86	90.54	63.26	85.13
Hierarchical Attention NN	71.36	77.89	66.15	88.93	74.28	64.68
LSTM	96.38	66.28	87.57	81.07	62.12	64.36
DCNN	70.02	82.93	90.86	63.92	70.21	66.46
Proposed	96.72	96.17	96.17	94.41	93.10	94.96

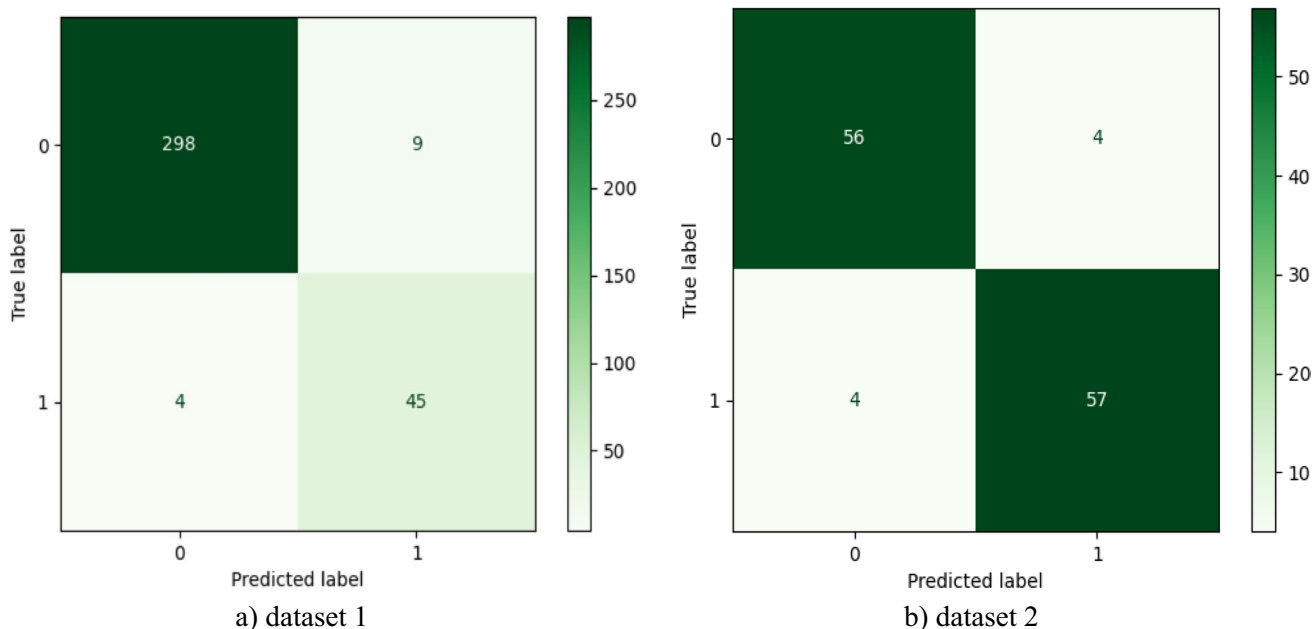


Fig. 9 Confusion matrix

labels are compared in which prostate cancer categories of 298 true positives (TP) and 45 true negatives (TN) are detected correctly which is highlighted in green shades and predicted less number of false positives (FP) and false negatives (FN) and reported as 9 and 4 respectively. Figure 9b in which the model predicted the tumor categories of 56

TP and 57 TN are detected correctly which is highlighted in green shades and predicted less number of FP and FN as 4 for dataset 2. Hence, the confusion matrix shows that the multilevel Bi-LSTM model is highly efficient in identifying and localizing prostate cancer.

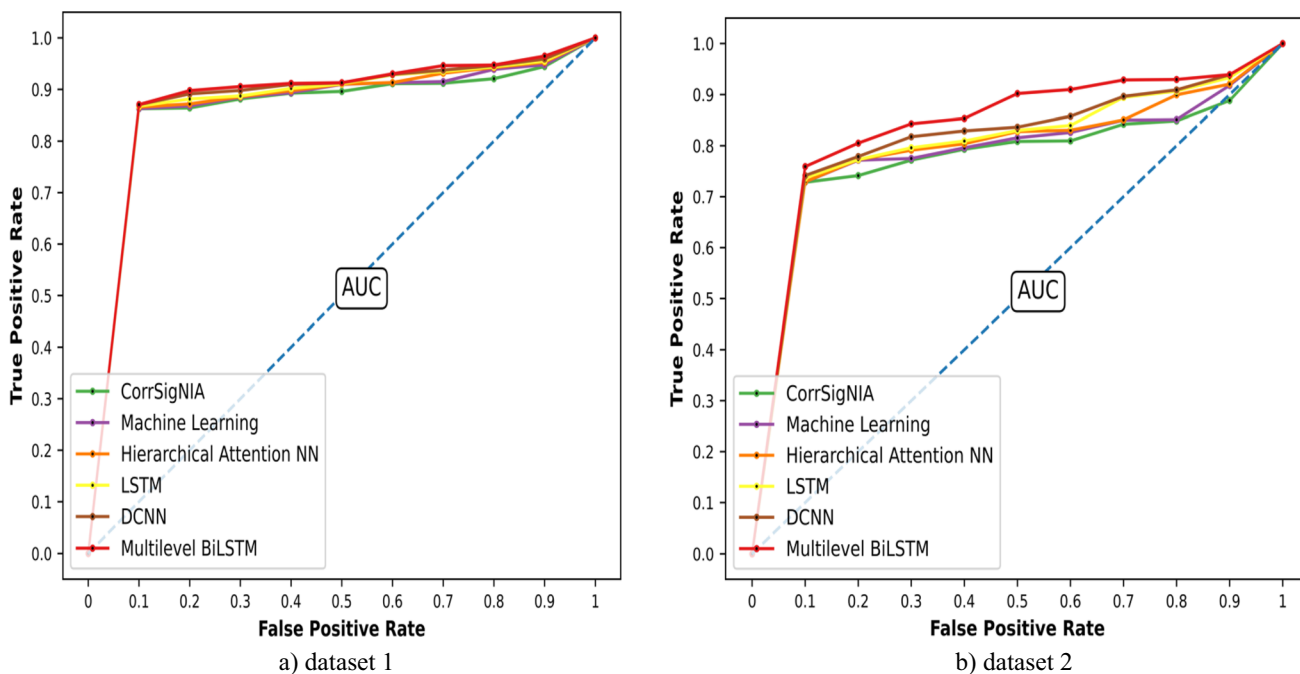


Fig. 10 ROC plot

ROC Plot

ROC illustrates the performance of the classifier model at varying threshold values. Figure 10a represents the ROC curve of dataset 1, in which the multilevel Bi-LSTM model predicted the false positive rate (FPR) and the corresponding true positive rates (TPR) for the training percentage to be varied from 10 to 90% and the proposed method obtained the ROC values of 0.87 at 0.1 FPR and TPR, ROC of 0.89 at 0.2 FPR and TPR, and the ROC values of 0.90, 0.91, 0.91, 0.93, 0.94, 0.94, 0.96, and 1 at FPR and TPR values of 0.3, 0.4, 0.5, 0.6, 0.7, 0.8, 0.9, and 1 respectively that proves the efficiency of the multilevel Bi-LSTM model with other techniques.

Conclusion

This study introduces an exhaustive framework designed for the accurate detection and localization of prostate cancers, spanning across the spectrum of aggressiveness, employing an intricate multilevel Bi-LSTM model. The workflow commences with the acquisition of MRI-based prostate cancer images from two prominent datasets, Prostate158—Training data and the Prostate MRI dataset, followed by meticulous pre-processing and ROI extraction. The pre-processed images undergo a multilevel feature map-based U-Net segmentation, bolstered by ResNet-101 and a channel-based attention module for improved performance. Subsequently, segmented images undergo feature extraction, encompassing various feature types, including statistical features, a global hybrid-based feature map, and a ResNet-101 feature map. These extracted features are then fed into the multilevel Bi-LSTM model and further optimized through channel and spatial attention mechanisms. Rigorous testing on a distinct dataset demonstrates the model's effectiveness, with performance evaluated through key metrics. This framework represents a promising approach for enhancing the diagnosis and localization of prostate cancers, encompassing both indolent and aggressive cases. The performance of the developed multilevel Bi-LSTM model showcases remarkable results, achieving accuracy, sensitivity, and specificity values of 96.72%, 96.17%, and 96.17% for dataset 1, and 94.41%, 93.10%, and 94.96% for dataset 2. These results substantiate the superior efficiency of this model compared to alternative methods. Furthermore, the other hybrid optimization techniques can be integrated into the multilevel Bi-LSTM technique to boost the localization of prostate cancer in the future.

Support Acknowledgements

The author would like to thank Omar Mohammed, MD for reviewing this manuscript.

Acknowledgements The author would like to thank the Deanship of Scientific Research at Shaqra University for supporting this work.

Data Availability The dataset used in this study is available publicly.

Declarations

Competing Interest The author declares no competing interests.

References

- Feng, Yujie, Fan Yang, Xichuan Zhou, Yanli Guo, Fang Tang, Fengbo Ren, Jishun Guo, and Shuiwang Ji. "A deep learning approach for targeted contrast-enhanced ultrasound-based prostate cancer detection." *IEEE/ACM Transactions on Computational Biology and Bioinformatics* 16, no. 6 (2018): 1794–1801.
- Iqbal, Saqib, Ghazanfar Farooq Siddiqui, Amjad Rehman, Lal Hussain, Tanzila Saba, Usman Tariq, and Adeel Ahmed Abbasi. "Prostate cancer detection using deep learning and traditional techniques." *IEEE Access* 9 (2021): 27085–27100.
- Arif, Muhammad, Ivo G. Schoots, Jose Castillo Tovar, Chris H. Bangma, Gabriel P. Krestin, Monique J. Roobol, WiroNiessen, and Jifke F. Veenland. "Clinically significant prostate cancer detection and segmentation in low-risk patients using a convolutional neural network on multi-parametric MRI." *European Radiology* 30 (2020): 6582–6592.
- Abbasi, Adeel Ahmed, Lal Hussain, Imtiaz Ahmed Awan, Imran Abbasi, Abdul Majid, Malik Sajjad Ahmed Nadeem, and Quratul-Ain Chaudhary. "Detecting prostate cancer using deep learning convolution neural network with transfer learning approach." *Cognitive Neurodynamics* 14 (2020): 523–533.
- Chen, Yingna, Chengdang Xu, Zhaoyu Zhang, Anqi Zhu, Xixi Xu, Jing Pan, Ying Liu, Denglong Wu, Shengsong Huang, and Qian Cheng. "Prostate cancer identification via photoacoustic spectroscopy and machine learning." *Photoacoustics* 23 (2021): 100280.
- Bhattacharya, Indrani, Arun Seetharaman, Christian Kunder, Wei Shao, Leo C. Chen, Simon JC Soerensen, Jeffrey B. Wang et al. "Selective identification and localization of indolent and aggressive prostate cancers via CorrSigNIA: an MRI-pathology correlation and deep learning framework." *Medical Image Analysis* 75 (2022): 102288.
- de Vente, Coen, Pieter Vos, MatinHosseinzadeh, JosienPluim, and MitkoVeta. "Deep learning regression for prostate cancer detection and grading in bi-parametric MRI." *IEEE Transactions on Biomedical Engineering* 68, no. 2 (2020): 374–383.
- Broomfield, Joseph, MelpomeniKalofonou, Sylvia Franklin, Sue M. Powell, Thomas Pataillot-Meakin, Nicolas Moser, Charlotte L. Bevan, and Pantelis Georgiou. "Handheld ISFET Lab-on-Chip detection of TMPRSS2-ERG and AR mRNA for prostate cancer prognostics." *IEEE Sensors Letters* (2023).
- Prostate158 - Training data <https://zenodo.org/record/6481141#.Y2TN73ZBy3A> accessed on October 2023.

10. Prostate MRI dataset <https://www.medicaldata.cloud/data-sets/prostate-mri-dataset/> accessed on October 2023.
11. Seetharaman, Arun, Indrani Bhattacharya, Leo C. Chen, Christian A. Kunder, Wei Shao, Simon JC Soerensen, Jeffrey B. Wang et al. “Automated detection of aggressive and indolent prostate cancer on magnetic resonance imaging.” *Medical Physics* 48, no. 6 (2021): 2960–2972.
12. Garcia-Marques, Fernando, Shiqin Liu, Sarah M. Totten, Abel Bermudez, Cheylene Tanimoto, En-Chi Hsu, Rosalie Nolley et al. “Protein signatures to distinguish aggressive from indolent prostate cancer.” *The Prostate* 82, no. 5 (2022): 605–616.
13. Duan, Heying, and Andrei Iagaru. “The use of advanced imaging in guiding the further investigation and treatment of primary prostate cancer.” *Cancer Imaging* 22, no. 1 (2022): 1–12.
14. Hennigan, S. Thomas, Shana Y. Trostel, Nicholas T. Terrigino, Olga S. Voznesensky, Rachel J. Schaefer, Nichelle C. Whitlock, Scott Wilkinson et al. “Low abundance of circulating tumor DNA in localized prostate cancer.” *JCO precision oncology* 3 (2019): 1–13.
15. Cheng, Pi-Wan, Samuel Davidson, and Ganapati Bhat. “Markers of malignant prostate cancer cells: Golgi localization of α -mannosidase 1A at GM130-GRASP65 site and appearance of high mannose N-glycans on cell surface.” *Biochemical and biophysical research communications* 527, no. 2 (2020): 406–410.
16. Eickelschulte, Samaneh, Anja Lisa Riediger, Arlou Kristina Angeles, Florian Janke, Stefan Duensing, Holger Sülmann, and Magdalena Görtz. “Biomarkers for the Detection and Risk Stratification of Aggressive Prostate Cancer.” *Cancers* 14, no. 24 (2022): 6094.
17. Dillinger, T., Sheibani-Tezerji, R., Pulverer, W., Stelzer, I., Hassler, M.R., Scheibelreiter, J., Pérez Malla, C.U., Kuroll, M., Domazet, S., Redl, E. and Ely, S., 2022. Identification of tumor tissue-derived DNA methylation biomarkers for the detection and therapy response evaluation of metastatic castration resistant prostate cancer in liquid biopsies. *Molecular Cancer*, 21(1), pp.1–8.
18. Moroianu, Ștefania L., Indrani Bhattacharya, Arun Seetharaman, Wei Shao, Christian A. Kunder, Avishkar Sharma, Pejman Ghanouni, Richard E. Fan, Geoffrey A. Sonn, and Mirabela Rusu. “Computational Detection of Extraprostatic Extension of Prostate Cancer on Multiparametric MRI Using Deep Learning.” *Cancers* 14, no. 12 (2022): 2821.
19. Rangel-Pozzo, Aline, Songyan Liu, Gabriel Wajnberg, Xuemei Wang, Rodney J. Ouellette, Geoffrey G. Hicks, Darrel Drachenberg, and Sabine Mai. “Genomic analysis of localized high-risk prostate cancer circulating tumor cells at the single-cell level.” *Cells* 9, no. 8 (2020): 1863.
20. Bhattacharya, Indrani, David S. Lim, Han Lin Aung, Xingchen Liu, Arun Seetharaman, Christian A. Kunder, Wei Shao et al. “Bridging the gap between prostate radiology and pathology through machine learning.” *Medical Physics* 49, no. 8 (2022): 5160–5181.
21. Cuocolo, Renato, Maria Brunella Cipullo, Arnaldo Stanzione, Lorenzo Ugga, Valeria Romeo, Leonardo Radice, Arturo Brunetti, and Massimo Imbriaco. “Machine learning applications in prostate cancer magnetic resonance imaging.” *European radiology experimental* 3, no. 1 (2019): 1–8.
22. Zhu, Lina, Ge Gao, Yi Zhu, Chao Han, Xiang Liu, Derun Li, Weipeng Liu et al. “Fully automated detection and localization of clinically significant prostate cancer on MR images using a cascaded convolutional neural network.” *Frontiers in Oncology* 12 (2022): 958065.
23. Jones, Abby L., Lasangi Dhanapala, Thaís A. Baldo, Mohamed Sharafeldin, Colleen E. Krause, Min Shen, Shirin Moghaddam et al. “Prostate cancer diagnosis in the clinic using an 8-protein biomarker panel.” *Analytical Chemistry* 93, no. 2 (2020): 1059–1067.
24. Toth, Reka, Heiko Schiffmann, Claudia Hube-Magg, Franziska Büscheck, Doris Höflmayer, Sören Weidemann, Patrick Lebok et al. “Random forest-based modelling to detect biomarkers for prostate cancer progression.” *Clinical epigenetics* 11 (2019): 1–15.
25. Mohammed, Siham A., Sadeq Darrab, Salah A. Noaman, and Gunter Saake. “Analysis of breast cancer detection using different machine learning techniques.” In *Data Mining and Big Data: 5th International Conference, DMBD 2020, Belgrade, Serbia, July 14–20, 2020, Proceedings 5*, pp. 108–117. Springer Singapore, 2020.
26. Barata, Catarina, Jorge S. Marques, and M. Emre Celebi. “Deep attention model for the hierarchical diagnosis of skin lesions.” In *Proceedings of the IEEE/CVF Conference on Computer Vision and Pattern Recognition Workshops*, pp. 0–0. 2019.
27. Gao, Riqiang, Yuankai Huo, Shunxing Bao, Yucheng Tang, Sanja L. Antic, Emily S. Epstein, Aneri B. Balar et al. “Distanced LSTM: time-distanced gates in long short-term memory models for lung cancer detection.” In *Machine Learning in Medical Imaging: 10th International Workshop, MLMI 2019, Held in Conjunction with MICCAI 2019, Shenzhen, China, October 13, 2019, Proceedings 10*, pp. 310–318. Springer International Publishing, 2019.
28. Thilagaraj, M., N. Arunkumar, and Petchinathan Govindan. “Classification of breast cancer images by implementing improved dcnn with artificial fish school model.” *Computational Intelligence and Neuroscience* 2022 (2022).
29. Gavade, A.B., Nerli, R., Kanwal, N., Gavade, P.A., Pol, S.S. and Rizvi, S.T.H., 2023. Automated diagnosis of prostate cancer using mpMRI images: A deep learning approach for clinical decision support. *Computers*, 12(8), p.152.
30. Alshareef, A.M., Alsini, R., Alsieni, M., Alrowais, F., Marzouk, R., Abunadi, I. and Nemri, N., 2022. Optimal deep learning enabled prostate cancer detection using microarray gene expression. *Journal of Healthcare Engineering*, 2022.
31. Ma, C., Lin, C., Samuel, O.W., Guo, W., Zhang, H., Greenwald, S., Xu, L. and Li, G., 2021. A bi-directional LSTM network for estimating continuous upper limb movement from surface electromyography. *IEEE Robotics and Automation Letters*, 6(4), pp.7217–7224.
32. Abass, Y.A. and Adeshina, S.A., 2021. Feature Selection with Ensemble Learning for Prostate Cancer Prediction from Gene Expression. *International Journal of Computer Science & Network Security*, 21(12spc), pp.526–538.
33. Yan, C., Fan, X., Fan, J. and Wang, N., 2022. Improved U-Net remote sensing classification algorithm based on Multi-Feature Fusion Perception. *Remote Sensing*, 14(5), p.1118.
34. Zhao, S., Shadabfar, M., Zhang, D., Chen, J. and Huang, H., 2021. Deep learning-based classification and instance segmentation of leakage-area and scaling images of shield tunnel linings. *Structural Control and Health Monitoring*, 28(6), p.e2732.
35. Mou, L., Zhao, Y., Chen, L., Cheng, J., Gu, Z., Hao, H., Qi, H., Zheng, Y., Frangi, A. and Liu, J., 2019. CS-Net: Channel and spatial attention network for curvilinear structure segmentation. In *Medical Image Computing and Computer Assisted Intervention–MICCAI 2019: 22nd International Conference, Shenzhen, China, October 13–17, 2019, Proceedings, Part I 22* (pp. 721–730). Springer International Publishing.
36. Kassem, M.A., Naguib, S.M., Hamza, H.M., Fouda, M.M., Saleh, M.K. and Hosny, K.M., 2023. Explainable Transfer Learning-Based Deep Learning Model for Pelvis Fracture Detection. *International Journal of Intelligent Systems*, 2023.
37. Eltoukhy, M.M., Hosny, K.M. and Kassem, M.A., 2022. Classification of multiclass histopathological breast images using residual deep learning. *Computational Intelligence and Neuroscience*, 2022.
38. Naguib, S.M., Hamza, H.M., Hosny, K.M., Saleh, M.K. and Kassem, M.A., 2023. Classification of Cervical Spine Fracture and Dislocation Using Refined Pre-Trained Deep Model and Saliency Map. *Diagnostics*, 13(7), p.1273.

39. Alshafi, Y.S., Kassem, M.A. and Hosny, K.M., 2023. Skin-Net: a novel deep residual network for skin lesions classification using multilevel feature extraction and cross-channel correlation with detection of outlier. *Journal of Big Data*, 10(1), p.105.

Springer Nature or its licensor (e.g. a society or other partner) holds exclusive rights to this article under a publishing agreement with the author(s) or other rightsholder(s); author self-archiving of the accepted manuscript version of this article is solely governed by the terms of such publishing agreement and applicable law.

Publisher's Note Springer Nature remains neutral with regard to jurisdictional claims in published maps and institutional affiliations.